Journal of the European Ceramic Society 20 (2000) 1803–1808

Phase formation and microstructural evolution of Ca α-sialon using different Si_3N_4 starting powders

Ya-Wen Li [a], Pei-Ling Wang [a,*], Wei-Wu Chen [a], Yi-Bing Cheng [b], Dong-Sheng Yan [a]

[a] *The State Key Lab of High Performance Ceramics and Superfine Microstructure, Shanghai Institute of Ceramics, CAS, Shanghai 200050, People's Republic of China*

[b] *Department of Materials Engineering, Monash University, Clayton, Victoria, 3168, Australia*

Received 14 September 1999; received in revised form 30 January 2000; accepted 16 February 2000

Abstract

Silicon nitride has two polymorphous structures, α-Si_3N_4 and β-Si_3N_4. In this study three different Si_3N_4 starting powders (~100%α, 40%α + 60%β, ~100%β) were used to prepare Ca α-sialon with the composition $Ca_{1.8}Si_{6.6}Al_{5.4}O_{1.8}N_{14.2}$ by pressureless sintering. Comparison was made concerning the densification process, reaction sequence and microstructure of the corresponding materials. The sluggish reactivity of β-Si_3N_4 resulted in poorer densification during sintering. All the three starting powders produced a similar final phase assembly, namely α-sialon together with a small amount of AlN and AlN polytypoid except that traces of unreacted β-Si_3N_4 remained until 1800° in samples prepared with ~100%β-Si_3N_4 powders. Elongated α-sialon grain morphology has been identified in the samples prepared using all the three different Si_3N_4 starting powders. Coarser elongated α-sialon grains with lower aspect ratio were found in samples using higher β phase starting powders.

Keywords: Microstructure-final; Phase equilibria; Sialons; Sintering; Si_3N_4

1. Introduction

α-Sialon is the solid solution of α-Si_3N_4 with the general formula expressed as $M_xSi_{12-(m+n)}Al_{(m+n)}O_nN_{16-n}$, where M represents calcium, lithium, magnesium, yttrium and most rare earth elements.[1] During the past decade, α-sialon has been most extensively studied in the yttrium and rare earth doped systems because of the high refractoriness of their boundary glass.[2] Recent study has revealed some advantages exclusively for Ca α-sialon, such as high solubility limit,[3,4] high thermal stability,[5] and the ease to evolve into elongated grain morphology.[6] All these features make Ca α-sialon an important system in the research of new structural ceramics possessing both high hardness and high toughness.

Previous study on rare earth sialon systems has frequently found an equi-axed grain morphology for the α-sialon phase,[7] which is also believed to be the reason for its relatively lower toughness and reliability comparing to β-sialon. Recent experimental findings of elongated α-sialon grains, especially the subsequent toughness enhancement to the material,[8,9] have aroused great interests among researchers for better understanding of the formation mechanism and hence better control of the elongated α-sialon. Up to now this objective has not been satisfactorily achieved.

According to Chen and Rosenflanz, overabundance of nucleation for α-sialon grains during sintering is the main reason for the scarce occurrence of elongated α-sialon.[8] They circumvented this problem by using β-Si_3N_4 as a starting powder and obtained elongated α-sialon grains in rare earth doped systems. Other studies have, however, shown that elongated α-sialon grains can also appear in the samples prepared from the α-Si_3N_4 powder.[9,10] It is therefore of interest to make clear the effect of Si_3N_4 starting powders on the microstructure of α-sialon. On the other hand, the densification process and reactions among different components during sintering would undoubtedly exert influence on the final α-sialon grain morphology. In this paper three Si_3N_4 starting powders with different α contents were employed to prepare Ca α-sialons with a fixed composition. Comparison was made concerning densification, phase evolution and microstructural development of the materials.

* Corresponding author.
E-mail address: plwang@sunm.shcnc.ac.cn (Pei-Ling Wang).

0955-2219/00/$ - see front matter
PII: S0955-2219(00)00058-3

2. Experimental

Specimens with a nominal composition of 1.8CaO:2.2Si_3N_4:5.4AlN (in mol ratio) were prepared by pressureless sintering. Three different Si_3N_4 starting powders were used as listed in Table 1. The corresponding specimens were designated as C180A (using ~100%α powders), C180B (using 40%α + 60%β powders) and C180C (using ~100%β powders). Same amounts of AlN (1.2 wt% O, China) and $CaCO_3$ (99.0%, China) were also added according to the designed composition. Proportioned powders were mixed in an agate mortar with alcohol for 2 h. Powders were uniaxially pressed into pellets at 5 MPa before cold isostatically pressed at 200 MPa. Sintering was carried out with flowing nitrogen as protective atmosphere in a graphite resistance furnace. A holding of 0.5 h at 1150°C was made to decompose $CaCO_3$ in the starting powders. Cooling took place inside the furnace by switching off the power after 2 h holding at the final sintering temperatures.

Bulk density was measured according to the Archimedes principle. Phase identification was performed on an RAX-10 diffractometer using CuK_α radiation. Semiquantitative analysis was made on the crystalline phase contents based on the calibration curves. XRD patterns were also obtained in a Guinier–Hägg camera (Cu $K_{\alpha 1}$ radiation, $\lambda = 1.5405981$ Å) using Si as an internal standard. With the aid of a computer-linked scanner (LS-18) system and corresponding programs,[11,12] cell parameters of α-sialon in selected samples were precisely determined. Microstructural observation was carried out on a KYKY-2000 scanning electron microscope (KY Inc, China) equipped with an energy dispersive spectrometer (Link ISIS 3.00). Polished surfaces of the prepared samples were etched in molten NaOH and carbon coated prior to observation.

3. Results and discussion

3.1. Densification behavior and reaction sequence

The densification process of pressureless sintered Ca α-sialon can be estimated from the density–temperature curve as shown in Fig. 1. The density of samples at nearly all the investigated temperatures follows the sequence as C180A > C180B > C180C. This is easily understood since β-Si_3N_4 is known to possess higher stability than α-Si_3N_4,[13] which retards its dissolution into the transient liquid, thus delaying densification. Therefore, the sluggish reactivity of β-Si_3N_4 resulted in lower density as well as later shrinkage in the samples containing higher β phase starting powders, which is more obvious in sample C180C.

Along with the densification process is the reaction among components. Using different Si_3N_4 starting powders did not significantly affect the final phase assembly, but there existed detectable differences in the phase development, as is evident in Fig. 2. With increasing temperature, the content of Si_3N_4 and AlN starting powders gradually decreased while the content of α-sialon gradually increased. Gehlenite ($Ca_2Al_2SiO_7$, or more likely a nitrogen containing compound $Ca_2Al_{2-x}Si_{1+x}O_{7-x}N_x$ as verified by the slight peak shift in the corresponding XRD film data) was the only intermediate phase, appearing as early as 1250°C and disappearing at 1650°C. The final phase assembly was α-sialon together with small amount of AlN polytypoid except that trace amount of unreacted β-Si_3N_4 remained in sample C180C sintered at 1800°C. However, a further increase of the sintering temperature at 1825°C led to complete dissolution of β-Si_3N_4 (see Fig. 2c).

The differences in the reaction sequence of the three samples were mainly reflected in the temperatures for complete dissolution of nitride starting powders and relative content of each phase. α-Si_3N_4 completely disappeared as early as 1550°C, whereas dissolution of β-Si_3N_4 required a much higher temperature (1825°C). At temperatures lower than 1450°C, the α-sialon content followed the sequence C180A > C180B > C180C. At temperatures exceeding 1450°C, with the dissolution of Gehlenite and Si_3N_4 in all the three samples, the α-sialon content increased, especially at 1550°C for C180A and C180B and 1650°C for C180C respectively. AlN polytypoid was the only crystalline phase in the final phase assembly

Table 1
Characteristics of the three Si_3N_4 starting powders

Type	Source	α Content (wt%)	Mean particle size (μm)
Si_3N_4-A	UBE E10, Japan	95	0.4
Si_3N_4-B	Lab-made (SHS)	40	0.6
Si_3N_4-C	Lab-made (SHS)	3	0.5

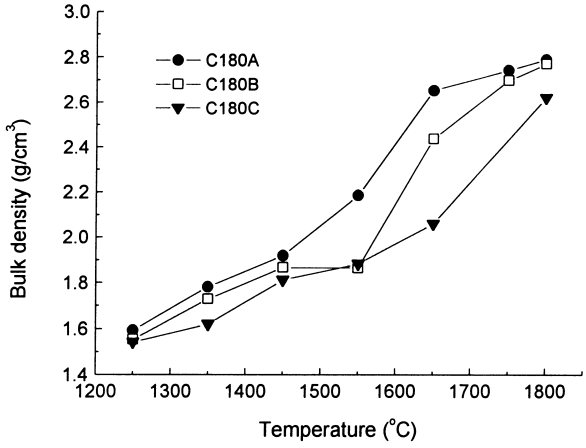

Fig. 1. Bulk density of Ca α-sialon using different Si_3N_4 starting powders pressureless sintered at different temperatures.

besides α-sialon. The occurrence of this phase accords with the recently established phase relationship on the two-dimensional Ca α-sialon plane,[14] which identified the phase compatibility triangles between α-sialon and AlN polytypoids for high x compositions. Close inspection of Fig. 2 revealed a systematic difference concerning the relative content of AlN polytypoid. The content of AlN polytypoid in Sample C180C remained at a relatively low level (~5 wt%), which is in contrast to the high value in Sample C180A (~17 wt%) and C180B (~19 wt%). Precise determination of the α-sialon cell dimensions in the 1800°C sintered samples (see Table 2) showed that C180C had a slightly smaller α-sialon cell at 1800°C comparing to C180A and C180B, which might be correlated with the incomplete reaction of C180C at this temperature. However, when β-Si_3N_4 completely disappeared after sintering at 1825°C, an obviously larger α-sialon cell was detected, indicating accommodation of more Al and Ca into the α-sialon lattice. This accords with the low AlN polytypoid content in the final phase assembly of C180C. Furthermore, the different AlN polytypoid content in the reaction sequence reflects the different AlN concentration in the transient liquid of the three samples, which may affect the grain growth and hence the final microstructure, as will be discussed below.

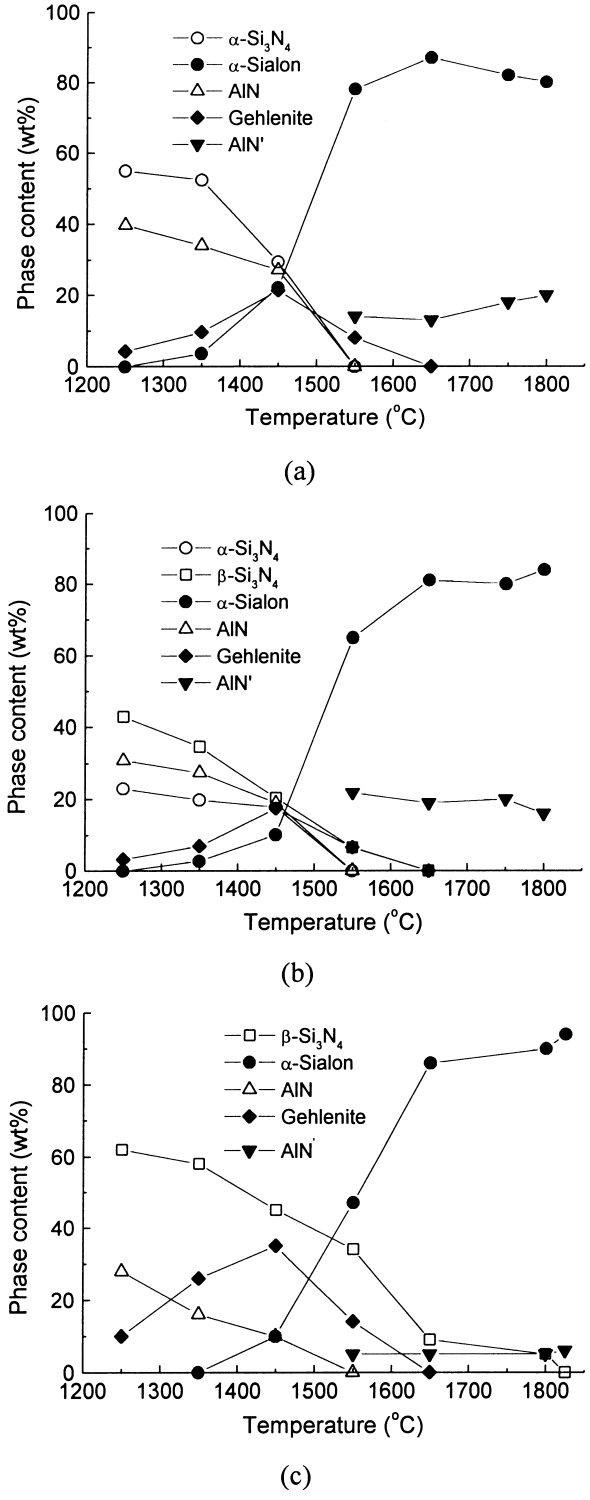

Fig. 2. Phase assembly of Ca α-sialon using different Si_3N_4 starting powders pressureless sintered at different temperatures: (a) C180A, (b) C180B, (c) C180C. Note: AlN′ denotes AlN polytypoid.

3.2. Microstructural development

Figs. 3 and 4 are SEM micrographs of pressureless sintered Ca α-sialon using three different Si_3N_4 starting powders at 1650 and 1800°C, respectively. The small grains in Fig. 3 are mostly spherical or roundish with aspect ratio no more than 2. This is in sharp contrast to Fig. 4, where elongated grains with aspect ratio higher than 5 are predominant in each image. The extraordinarily large plate-like grains belong to the AlN-polytypoid phase.[15] Obvious difference in the three samples sintered at the two temperatures could also be detected concerning the grain density and aspect ratio of α-sialon. Sample C180A had the highest particle density and sample C180C the lowest. On the other hand, the aspect ratio of α-sialon grains in sample C180A was obviously higher than that in sample C180C shown in Fig. 4.

It has been generally accepted that the elongated grain morphology of β-Si_3N_4 and β-sialon resulted from their hexagonal structure.[16] Extensive studies have been carried out to understand the mechanism for this anisotropic grain growth behavior. Like its β counterpart,

Table 2
Cell dimensions of α-sialon pressureless sintered at 1800°C using different Si_3N_4 starting powders

	a	c	V
C180A	7.8849(6)	5.7337(5)	308.72
C180B	7.8806(6)	5.7261(6)	307.97
C180C	7.875(1)	5.729(2)	307.66
C180C*[a]	7.8985(6)	5.7406(8)	310.15

[a] The cell dimensions of C180C* are taken from the 1825°C sintered sample.

α-sialon also has a hexagonal structure with the *c* axis shorter than the *a* axis. The occurrence of elongated shape of α-sialon grains may thus be regarded as an indication of its intrinsic morphology. The different microstructures of the samples using different Si_3N_4 powders provide some clue to understand the nucleation and growth mechanism of elongated α-sialon.

As is known, densification of sialon ceramics is effected through the liquid phase sintering, along with which the sialon phases also form through the nucleation and grain growth process. Most previous studies have observed heterogeneous nucleation of α-sialon and β-sialon, though the possibility of homogeneous nucleation from the supersaturated liquid phase can not be totally excluded, as illustrated in Hwang's work.[17,18] For the present Ca sialon composition, due to the much higher Gibbs free energy required in the formation of nuclei for homogeneous nucleation than for heterogeneous nucleation and to the existence of abundant foreign particles throughout the sintering process, heterogeneous nucleation should be a more possible mechanism for α-sialon. In other words, the undissolved Si_3N_4, AlN and even the intermediate phase gehlenite can serve as possible

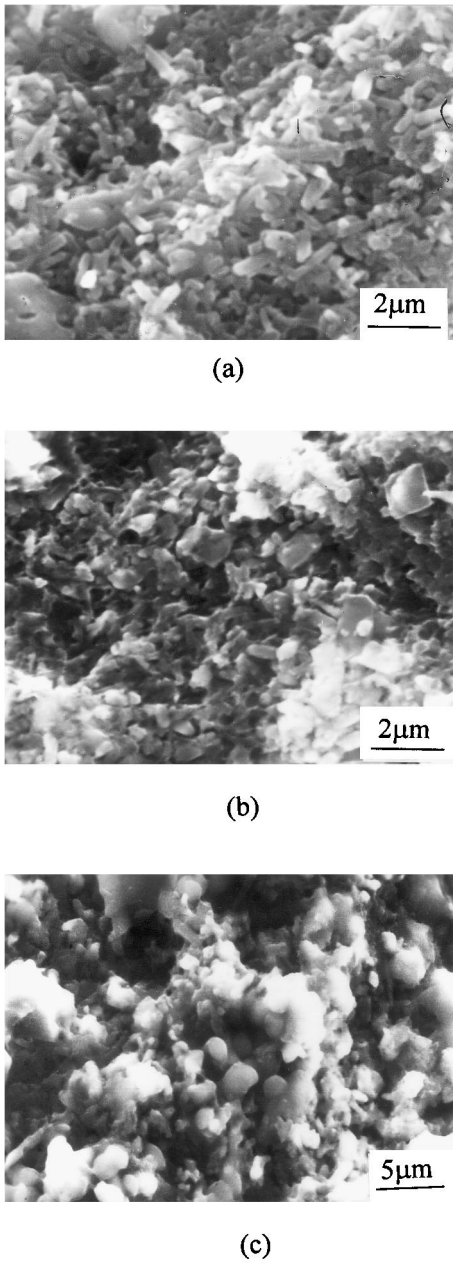

Fig. 3. SEM micrograph of Ca α-sialon using different Si_3N_4 starting powders after pressureless sintering at 1650°C for 2 h: (a) C180A, (b) C180B, (c) C180C.

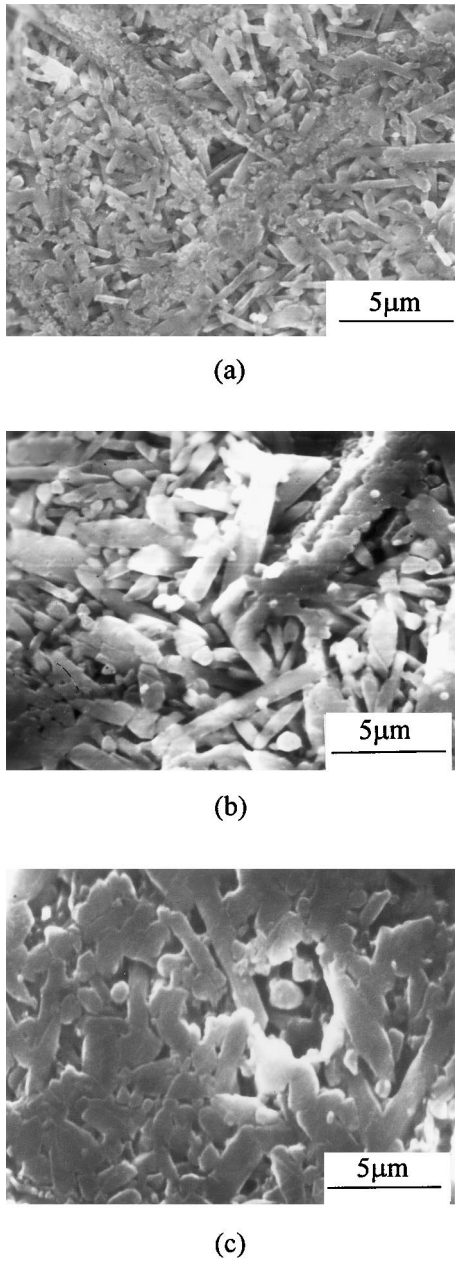

Fig. 4. SEM micrograph of Ca α-sialon using different Si_3N_4 starting powders after pressureless sintering at 1800°C for 2 h. The extraordinarily large plate-like grains in the figure belong to the AlN-polytypoid phase: (a) C180A, (b) C180B, (c) C180C.

nucleation sites for α-sialon. It is also easy to understand then that because of the similarity in both structure and composition between α-sialon and α-Si_3N_4, nucleation of α–sialon on α-Si_3N_4 should be energetically more favorable than nucleation of α-sialon on β-Si_3N_4 or other phases. A higher nucleation rate of α-sialon on α-Si_3N_4 could therefore be expected according to the formula:[19]

$$I_{het} = \frac{A_c T}{\eta} \exp\left(-W^*_{het}/kT\right) \quad (1)$$

where I_{het} the heterogeneous nucleation rate, $A_c = n_v k/3\pi\lambda^3$, with n_v the formula units of the crystallizing component phase per unit volume of the liquid, k the Boltzmann constant, λ the quantity of the order of the atomic dimensions (''jump distance''), η the viscosity of the liquid and W_{het}* the Gibbs free energy to form a critical nucleus (thermodynamic barrier). Thus the higher α-Si_3N_4 phase content in the starting composition, the more favorable it is for the nucleation of α-sialon. This is in accordance with the much higher grain density in sample C180A than in C180C. It is further concluded that overabundance of α-sialon nucleation can be overcome by using higher β-Si_3N_4 phase powders, which agrees with Chen's recent work.[8]

Nevertheless, the occurrence of elongated α-sialon in both samples C180A and C180C at 1800°C seems to contradict Chen's claim that ''overabundance of nucleation is the main reason for the scarce occurrence of elongated α-sialon''. Moreover, the grain aspect ratios of α-sialon in the three samples show the sequence of C180A > C180B > C180C, as is more obvious in the pore region of the sintered compacts (see Fig. 5). This suggests that the nucleation density should not be the only factor in determining the α-sialon grain morphology. Rather, some other factors, such as the amount and viscosity of liquid during the grain growth process, might play a more important role. Our previous observation on microstructure of Ca α-sialon has shown increasing aspect ratio and proportion of elongated α-sialon grains with increasing x value in the designed composition, which is believed to be due to the formation of more liquid during sintering.[20] The occurrence of elongated α-sialon grains in all the three samples, therefore, should be attributed to the high x composition chosen in this study.

As known from the XRD results, only α-sialon and AlN polytypoid were detected after sintering at 1650°C (C180C also contained a small amount of unreacted β-Si_3N_4), which indicates that the grain growth of α-sialon between 1650 and 1800°C could be categorized as Ostwald ripening by a dissolution/precipitation process via the transient liquid. Or, it might be more convenient to term it as ''secondary dissolution/precipitation'' to distinguish it from the primary process of phase transformation from α-Si_3N_4 to α-sialon. This analysis resembles that in the study of β-Si_3N_4 and β-sialon. There is, however, some distinction between the two cases. For example, the β grains after the α-β phase transformation were already elongated,[21,22] whereas nearly spherical α-sialon grains were observed after the α-α′ phase transformation (see Fig. 3). Accordingly, the mean aspect ratio with increasing temperatures was decreased for the β grains and increased for the α-sialon grains as shown in this study. It is therefore reasonable to expect a different grain growth mechanism during the Ostwald ripening. Our ongoing work is aiming at this objective.

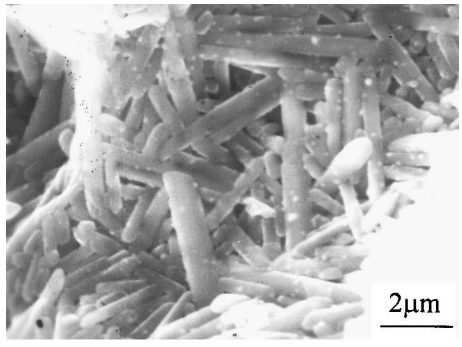

(a)

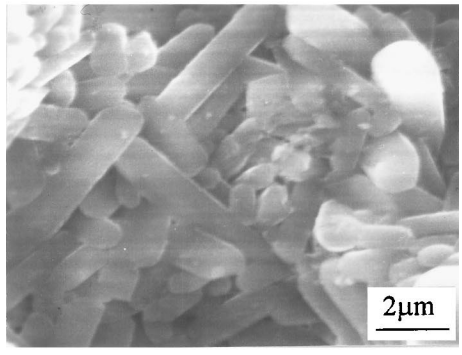

(b)

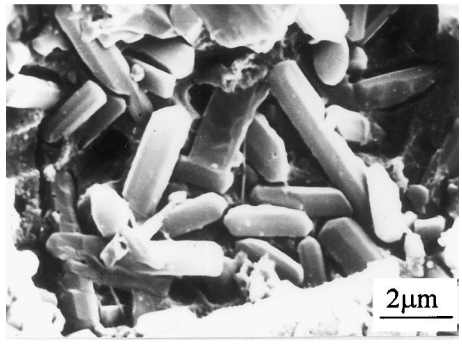

(c)

Fig. 5. SEM micrograph of Ca α-sialon using different Si_3N_4 starting powders in the pore region after pressureless sintering at 1800°C for 2 h: (a) C180A, (b) C180B, (c) C180C.

Whatever the underlying mechanism is for the grain growth of α-sialon, it is understandable that the amount and viscosity of the transient liquid could greatly influence the rate of atom transport, thus affecting the driving force for the grain growth. From the density–temperature curve (Fig. 1), sample C180C had the lowest densification rate as well as the lowest density, implying less transient liquid with higher viscosity formed during sintering for C180C. It is also known from the result of reaction sequence (Fig. 2) that the AlN polytypoid content was much lower in sample C180C than in C180A and C180B. Accordingly, the liquid of C180C was more AlN-rich during the grain growth period and had a higher viscosity (both Al and N are reported to increase the viscosity of oxynitride glass[23,24]). It is therefore reasonable to assume certain correlation between the less liquid with higher viscosity during sintering and the lower aspect ratio of α–sialon in the microstructure of C180C. The more viscous liquid formed in sample C180C could hinder the atom diffusion along the *c* axis, thus reducing the driving force for the anisotropic grain growth and giving rise to the lowest aspect ratio of α-sialon.

4. Conclusions

Due to the sluggish reactivity of β-Si_3N_4, Ca α-sialon compacts using β-Si_3N_4 starting powders showed a later shrinkage as well as a lower density. The final phase assembly of Ca α-sialon composition was not affected significantly by the different Si_3N_4 starting powders used except that traces of unreacted β-Si_3N_4 remained in the 1800°C sintered compact containing 100% β-Si_3N_4 starting powders. The occurrence of elongated α-sialon grain morphology in all the pressureless sintered samples with the three kinds of Si_3N_4 starting powders indicates that α-sialon could take its intrinsic elongated shape if grown under proper conditions. Higher β phase in the starting powders resulted in lower grain density of α-sialon with lower aspect ratio in the final microstructure, which reflects the influence of Si_3N_4 type on the nucleation and grain growth of α-sialon.

Acknowledgements

This work has received financial support from the National Natural Science Foundation of China. The authors would like to thank Dr. Bao-Lin Zhang in Shanghai Institute of Ceramics for providing the Si_3N_4 powders.

References

1. Hampshire, S., Park, H. K., Thompson, D. P. and Jack, K. H., α′-Sialon ceramics. *Nature*, 1978, **274**, 880–882.
2. Ekström, T. and Nygren, M., Sialon ceramics. *J. Am. Ceram. Soc.*, 1992, **75**, 259–276.
3. Jack, K. H., The characterization of α-sialons and the α-β relationships in sialons and silicon nitrides. In *Progress in Nitrogen Ceramics*, ed. F. L. Riley. Martinus Nijhoff, The Hague, Netherlands, 1983, pp. 45–49.
4. Huang, Z. K., Sun, W. Y. and Yan, D. S., Phase relations of the Si_3N_4–AlN–CaO system. *J. Mater. Sci. Lett.*, 1984, **4**, 255–259.
5. Hewett, C. L., Cheng, Y. B., Muddle, B. C. and Trigg, M. B., Thermal stability of calcium α-sialon ceramics. *J. Eur. Ceram. Soc.*, 1998, **18**, 417–427.
6. Zhao, H., Swenser, S. and Cheng, Y. B., Elongated α-sialon grains in pressureless sintered sialon ceramics. *J. Eur. Ceram. Soc.*, 1998, **18**, 1053–1057.
7. Tien, T. Y., Silicon nitride ceramics — alloy design. In *Silicon Nitride Ceramics Scientific and Technological Advances*, ed. I. W. Becher, P. H. Becher, M. Motomo, G. Petzow and T. S. Yen. MRS, Pittsburgh, PA, 1993, pp. 51–63.
8. Chen, I. W. and Rosenflanz, A., A tough sialon ceramic based on α-Si_3N_4 with a whisker-like microstructure. *Nature*, 1997, **389**, 701–704.
9. Wood, C., Zhao, H. and Cheng, Y.-B., Microstructural development of calcium α-sialon ceramics with elongated grains. *J. Am. Ceram. Soc.*, 1999, **82**, 421–428.
10. Shen, Z. J., Nordberg, L.-O., Nygren, M. and Ekstrm, T., α-Sialon grains with high aspect ratio — utopia or reality? In *Engineering Ceramics '96: Higher Reliability through Processing*, ed. G. N. Babini. Kluwer Academic Publishers, Netherlands, 1997, pp. 169–178.
11. Johansson, K. E., Palm, T. and Werner, P.-E., An automatic microdensitometer for X-ray powder diffraction photographs. *J. Phys. E.: Sci. Instrum*, 1980, **13**, 1289.
12. Werner, P.-E., A Fortran program for least-square refinement of crystal-structure cell dimensions. *Arkiv fur Kemi*, 1964, **31**, 513.
13. Mitomo, M. and Tajima, Y., Sintering, properties and applications of silicon nitride and sialon ceramics. *J. Ceram. Soc. Jpn*, 1991, **99**, 1014–1025.
14. Hewett, C. L., Cheng, Y. B., Muddle, B. C. and Trigg, T. B., Phase relationships and related microstructural observations in the Ca–Si–Al–O–N system. *J. Am. Ceram. Soc.*, 1998, **81**, 1781–1788.
15. Wang, P. L., Sun, W. Y. and Yan, D. S., Mechanical properties of AlN-polytypoids — 15R, 12H and 21R. *Mater. Sci. Eng.*, 1999, **A272**, 351–356.
16. Krammer, M., Wittmuss, D., Kuppers, H., Hoffmann, M. J. and Petzow, G., Relations between crystal structure and growth morphology of β-Si_3N_4. *J. Cryst. Growth*, 1994, **140**, 157–166.
17. Hwang, S.-L. and Chen, I-W., Nucleation and growth of α′-sialon on α-Si_3N_4. *J. Am. Ceram. Soc.*, 1994, **77**, 1711–1718.
18. Hwang, S.-L. and Chen, I-W., Nucleation and growth of β′-sialon. *J. Am. Ceram. Soc.*, 1994, **77**, 1719–1728.
19. James, P. F., Nucleation in glass-forming system — a review. In *Nucleation and Crystallization in Glasses*, ed. J. H. Simmons, D. R. Uhlmann and G. H. Beall. Am. Ceram. Soc. Inc, Columbus, Ohio, 1982, pp. 1–48.
20. Li, Y. W., Wang, P. L., Cheng, Y. B. and Yan, D. S., Microstructure and property anisotropy of hot-pressed Ca α–sialon. *J. Mater. Sci. Letters*, in press.
21. Kramer, M., Hoffmann, M. J. and Petzow, G., Grain growth studies of silicon nitride dispersed in an oxynitride glass. *J. Am. Ceram. Soc.*, 1993, **76**, 2778–2782.
22. Wotting, G., Kanka, B. and Ziegler, G., Microstructural development, microstructural characterization and relation to mechanical properties of dense silicon nitride.. In *Nonxide Technical and Engineering Ceramics*, ed. S. Hampshire. Elsevier Applied Science, London, 1986, pp. 83–96.
23. Hampshire, S., Drew, R. A. and Jack, K. H., Oxynitride glasses. *Phy. Chem. Glasses*, 1985, **26**, 182–186.
24. Scholze H., *Glas natur, struktur und eigenschaften*. Springer-Verlag, 1977, pp. 185–187.